

# Theoretical study of finite temperature spectroscopy in van der Waals clusters. I. Probing phase changes in $\text{CaAr}_n$

F. Calvo, F. Spiegelman and M.-C. Heitz

*Laboratoire de Physique Quantique, IRSAMC, Université Paul Sabatier,  
118 Route de Narbonne, F31062 Toulouse Cedex, France*

The photoabsorption spectra of calcium-doped argon clusters  $\text{CaAr}_n$  are investigated at thermal equilibrium using a variety of theoretical and numerical tools. The influence of temperature on the absorption spectra is estimated using the quantum superposition method for a variety of cluster sizes in the range  $6 \leq n \leq 146$ . At the harmonic level of approximation, the absorption intensity is calculated through an extension of the Gaussian theory by Wadi and Pollak [J. Chem. Phys. **110**, 11890 (1999)]. This theory is tested on simple, few-atom systems in both the classical and quantum regimes for which highly accurate Monte Carlo data can be obtained. By incorporating quantum anharmonic corrections to the partition functions and respective weights of the isomers, we show that the superposition method can correctly describe the finite-temperature spectroscopic properties of  $\text{CaAr}_n$  systems. The use of the absorption spectrum as a possible probe of isomerization or phase changes in the argon cluster is discussed at the light of finite-size effects.

## I. INTRODUCTION

Large van der Waals clusters offer a convenient medium to study solvation at the molecular level, and also to undertake chemical reactions with well defined thermodynamical conditions.<sup>1,2,3</sup> Reactivity of chromophore-doped rare-gas clusters has been the subject of intense experimental effort.<sup>4,5,6,7,8,9</sup> Photodissociation of HBr on argon clusters has been investigated by Baumfalk *et al.*,<sup>4,5,6</sup> including a theoretical study of the HBr-cluster interaction.<sup>5</sup> Chemiluminescence in the bimolecular reaction  $\text{Ba} + \text{N}_2\text{O} \rightarrow \text{BaO}^* + \text{N}_2$  was the subject of a work by Gaveau *et al.*,<sup>7</sup> and photodetachment in  $\text{IHI}^- \text{Ar}_n$  clusters was used to probe transition state spectroscopy of the  $\text{I} + \text{HI}$  reaction by Liu and coworkers.<sup>8</sup> One may also cite the photoinduced reaction dynamics between  $\text{Ca}^*$  and HBr towards  $\text{CaBr}^* + \text{H}$  at the surface of a large argon cluster carried out by Briant *et al.*<sup>9</sup> Very recently, the reaction between  $\text{N}_2\text{O}$  and  $\text{Li}_2$  mediated by  $\text{Ar}_n$  clusters has been investigated by Breckenridge and coworkers.<sup>10</sup>

A practical understanding of the physical and chemical properties of the deposited species relies on a good characterization of their spectroscopy. In turn, spectroscopy gives great insight into the structure of the van der Waals complex, especially in concern with the location of the chromophore.<sup>11,12,13</sup> This idea was used to propose a way of detecting structural transformations inside the cluster.<sup>14,15</sup> Not long after its was discovered in simulations,<sup>16</sup> the so-called dynamical coexistence phenomenon between solidlike and liquidlike phases received some experimental evidence by Hahn and Whetten who reported changes in the excitation spectrum of benzene-(argon)<sub>n</sub> clusters with increasing temperature.<sup>14</sup> Similar experimental results were reported for dichloroanthracene- $\text{Ar}_n$  clusters by Even *et al.*<sup>15</sup> More recently, Curotto and coworkers<sup>17,18,19</sup> theoretically investigated the infrared spectroscopy in  $\text{Ar}_n$ -HF clusters. They observed significant variations in the red shift associated with the two lowest vibrational states

of the HF molecule, which they could correlate with the thermodynamical state of the cluster.<sup>17,18,19</sup> Moseler *et al.*<sup>20</sup> found that the photoabsorption spectra of  $\text{Na}_8$  displays some features characteristic of isomerization and structural fluctuations. Lastly, simulations on charged rare-gas clusters have investigated the influence of temperature on the absorption spectrum.<sup>21,22</sup> So far, no direct evidence for isomerization in such rare-gas clusters has been found yet.

While spectroscopy has many attractive features for experimental studies in large clusters, several difficulties pave the way for efficient theoretical approaches. Firstly, because of the numerous degrees of freedom, a fully quantum calculation of the absorption spectrum by exact methods (wavepacket or diagonalization in a basis) is not feasible beyond a few atoms and one is usually lead to simplify the problem. A common approximation is the Condon hypothesis, which assumes vertical transitions. Secondly, the equilibrium properties at finite temperature require some sampling of the ground state potential energy surface (PES). This sampling can be hard to get because of the topography of the multidimensional PES (the so-called energy landscape). When the energy landscape is complicated or has multiple funnels, the relaxation to equilibrium may be particularly slow with a glassy-like behavior.<sup>23</sup> Broken ergodicity is then likely to occur in conventional molecular dynamics (MD) or Monte Carlo (MC) simulations, and also in quantum simulations. Fortunately some remedies to this problem have recently been suggested, including multi-canonical ensemble sampling<sup>24</sup> or parallel tempering.<sup>25</sup> Thirdly, most experiments involving chromophore-doped rare-gas clusters take place at low temperatures, at which the classical approximation may be questioned, especially for the lighter elements neon and helium. Path-integral Monte Carlo or centroid MD should then be used instead of classical techniques, however their use with ergodicity restoring strategies remains numerically demanding for systems containing tens or hundreds degrees of freedom.

We have recently proposed an alternative way of calculating thermodynamical observables at canonical equilibrium, using the superposition approximation of quantum oscillators.<sup>26</sup> This method, originally developed for thermodynamical observables only, was improved phenomenologically by including anharmonic corrections,<sup>26,27</sup> and extended to generally treat other temperature-dependent observables.<sup>28</sup> Its main interest is to circumvent the troubles of broken ergodicity by considering separately the contribution of each isomer to the partition function. The method also naturally describes quantum delocalization in a straightforward way.

One goal of this paper is to extend the quantum superposition method to the realm of calculating photoabsorption spectra. In addition to the ingredients presently available, one needs to calculate the photoabsorption spectra of each stable isomer. For this, we use a recent theory by Wadi and Pollak<sup>29</sup> that we have extended to the general case of arbitrary potential surfaces. As will be seen below, this Gaussian theory of absorption succeeds in predicting absorption line shapes, widths and shifts for harmonic polyatomic molecules in good agreement with highly accurate Monte Carlo data.

With the quantum superposition method, we are able to carry out systematic studies for a given set of cluster sizes. We can then address our second goal, and try to relate the features of the absorption spectrum to the knowledge of isomerizations and possible phase changes inside the cluster. More specifically, by looking at particular sizes we hope to gain insight in the relationship between structure, temperature, quantum delocalization, and the shape and position of the spectral lines.

This work follows previous efforts aimed at interpreting experimental absorption spectra on large CaAr<sub>n</sub> clusters.<sup>13</sup> The spectroscopy of the CaAr diatomic molecule has been investigated both experimentally and with *ab initio* calculations in Ref. 30, and a Diatomic-In-Molecules (DIM) Hamiltonian was constructed to model the 4s ground- and 4s4p excited-states of CaAr<sub>n</sub> clusters.<sup>13</sup> In the present context of finite-temperature spectroscopy, the heavy numerical cost of statistical sampling is balanced with this relatively cheap, albeit accurate Hamiltonian. The paper is organized as follows. In the next section, we briefly recall the quantum superposition method in the harmonic approximation. We also include the derivation of approximate perturbative anharmonic quantum corrections to the partition functions. The Gaussian theory of absorption for harmonic molecules, initially proposed by Wadi and Pollak,<sup>29</sup> will be generalized to include possible Duschinskii rotations in Sec. III. These methods will be tested on simple clusters, in both the classical and quantum regimes, by comparing their results to high statistics Monte Carlo data. Their main application to the variations of the photoabsorption spectrum with temperature in some size-specific CaAr<sub>n</sub> clusters will be presented in Sec. IV. The results will be discussed in view of the isomerization and phase changes phenomena. Some concluding remarks will close

the paper in Sec. V.

## II. QUANTUM SUPERPOSITION METHOD

In the superposition approach,<sup>31,32,33</sup> also known as the multiple normal modes model,<sup>34</sup> the total partition function  $Z$  of the  $N$ -atom system in equilibrium at temperature  $T = 1/k_B\beta$  is replaced by a sum over stable minima  $\{\alpha\}$ :

$$Z(\beta) = \sum_{\alpha} n_{\alpha} Z_{\alpha}(\beta). \quad (1)$$

Each minimum  $\alpha$ , or inherent structure, has a contribution  $Z_{\alpha}$  to  $Z$ , further weighted by the degeneracy factor  $n_{\alpha}$ , which accounts for permutational isomers and global symmetry. In CaAr<sub>n</sub> clusters ( $N = n + 1$ ),  $n_{\alpha}$  is given by  $2n!/h_{\alpha}$ , where  $h_{\alpha}$  is the order of the point group of structure  $\alpha$ . The problem has now been reduced to estimating the individual functions  $Z_{\alpha}$ . At the simplest level of approximation, the harmonic vibrational frequencies  $\{\omega_{\alpha i}\}$  provide a zero-th order expression for  $Z_{\alpha}$ :

$$Z_{\alpha}^{(0)}(\beta) = e^{-\beta E_{\alpha}} \prod_i \frac{2}{\sinh \beta \hbar \omega_{\alpha i} / 2}, \quad (2)$$

with  $\hbar$  the reduced Planck's constant and  $E_{\alpha}$  the potential energy minimum of isomer  $\alpha$ . In the classical regime  $\hbar \rightarrow 0$ , the decomposition (1) is formally exact, since each point of the configuration space (except saddle points) belong to one and only one basin  $\alpha$ . In the quantum regime (finite  $\hbar$ ), tunnelling is neglected.<sup>26</sup> In principle, the knowledge of all minima of the energy landscape allows us to calculate any thermodynamical observable, including internal energy and heat capacity, from Eq. (1). However, for all but the smallest atomic systems, exhaustive enumeration of these isomers is not possible because the number of local minima is thought to grow exponentially with the number of degrees of freedom.<sup>35</sup> To correct for the uncompleteness of the available set of isomers, a reweighting technique can be used.<sup>26,33</sup> The idea is to perform a simulation at a reference temperature  $T_0$ , and to compute the probability  $p_{\alpha}$  of observing isomer  $\alpha$ . The partition function  $Z$  is approximated as a *partial* sum over *weighted* isomers:

$$Z(\beta) \propto \sum'_{\alpha} g_{\alpha} n_{\alpha} Z_{\alpha}(\beta), \quad (3)$$

with the partial character of the sum indicated by the prime symbol. If we assume that the weights  $\{g_{\alpha}\}$  are independent of temperature, the probability  $p_{\alpha}(T_0)$  of finding isomer  $\alpha$  at  $T_0$  is proportional to  $g_{\alpha} n_{\alpha} Z_{\alpha}(\beta_0)$ . Hence,  $Z$  can be expressed as

$$Z(\beta) \propto \sum'_{\alpha} p_{\alpha}(\beta_0) \frac{Z_{\alpha}(\beta)}{Z_{\alpha}(\beta_0)}. \quad (4)$$

A classical simulation can be used to sample the minima and their respective weights.<sup>26</sup> In the above equation, the denominators  $Z_\alpha(\beta_0)$  should then be replaced by their classical analogue. Even though the resulting partition function (4) should not depend on the classical or quantum nature of the simulation, some differences can be seen when using semiclassical simulations including quantum corrections.<sup>28</sup> This reweighting procedure has been shown to improve significantly the predictions of the superposition method. In particular, Wales was able to obtain a 'S-bend' in the kinetic temperature of Ar<sub>55</sub>,<sup>33</sup> as seen previously in simulations.<sup>36</sup>

The other important limitation of the method is the harmonic approximation used to calculate  $Z_\alpha(\beta)$ . Several phenomenological anharmonic corrections have been proposed in the literature for classical systems.<sup>27,37</sup> In the case of quantum systems, the optimal normal modes method of Cao and Voth<sup>38</sup> can be used to include anharmonicity to some extent, but the self-consistency required makes it computationally heavy for large sets of isomers. Building upon a recent effort to include systematic corrections from the energy surface topography via classical perturbation theory,<sup>39</sup> we can attempt to include anharmonicities in the quantum partition functions  $Z_\alpha$  in a more rigorous fashion. Since the classical corrections are also numerically demanding, we restrict ourselves to low-order corrective terms. In order to make the reading easier, the details of the perturbation expansion are given in the Appendix. The superposition method not only provides the thermodynamical equilibrium properties, and other quantities can be computed provided they can be calculated for each minimum  $\alpha$ .<sup>28</sup> At thermal equilibrium, the average value  $\langle A \rangle$  of the global observable  $A$  is the weighted sum over minima:

$$\langle A \rangle(T) = \frac{\sum'_\alpha p_\alpha(T_0) Z_\alpha(T) A_\alpha(T) / Z_\alpha(T_0)}{\sum'_\alpha p_\alpha(T_0) Z_\alpha(T) / Z_\alpha(T_0)}. \quad (5)$$

### III. GAUSSIAN THEORY OF ABSORPTION

We assume that the cluster is in canonical equilibrium at temperature  $T = 1/k_B\beta$ , and that it undergoes an excitation by an infinitely narrow pulse at frequency  $\omega$  from its ground state potential surface  $V_g(\mathbf{R})$ . The normalized excitation spectrum  $\mathcal{I}(\omega, \beta)$  is<sup>40</sup>

$$\mathcal{I}(\omega, \beta) = \frac{\sum_i \sum_j \delta(\Delta E + E_{e_j} - E_{g_i} - \hbar\omega) e^{-\beta E_{g_i}} |\langle e_j | \mu | g_i \rangle|^2}{\sum_i \sum_j e^{-\beta E_{g_i}} |\langle e_j | \mu | g_i \rangle|^2} \quad (6)$$

with  $|g_i\rangle$  and  $|e_j\rangle$  the eigenstates with eigenenergies  $E_{g_i}$ ,  $E_{e_j}$  of the ground- and excited-state Hamiltonians  $H_g$  and  $H_e$ , respectively. The transition dipole moment  $\mu_{ij} = |\langle e_j | \mu | g_i \rangle|^2$  will be taken as constant in the usual Condon approximation of vertical excitations.  $\Delta E$  is the energy difference between the bottom of the ground- and excited-state surfaces. The absorption intensity can be

expressed as the Fourier transform of the imaginary-time correlation function:<sup>29</sup>

$$\mathcal{I}(\omega, \beta) = \frac{\hbar}{2\pi Z(\beta)} \int_{-\infty}^{\infty} \chi(\tau, \beta) e^{-i\tau(\Delta E - \hbar\omega)} d\tau, \quad (7)$$

with

$$\chi(\tau, \beta) = \text{Tr} \left[ e^{-i\tau H_e} e^{-(\beta - i\tau) H_g} \right], \quad (8)$$

and where  $Z(\beta) = \text{Tr} e^{-\beta H_g}$  is the partition function. Following Wadi and Pollak,<sup>29</sup> we now perform a short-time expansion in the correlation function. This expansion should be valid at moderate temperatures and for a large number of degrees of freedom. Indeed, in such cases the combination of the numerous vibrational modes will significantly dephase rapidly, and the correlation function will be nonzero only for short times. Using this approximation, the absorption intensity can be calculated analytically<sup>29</sup> as a Gaussian function:

$$\mathcal{I}(\omega, \beta) = \frac{\hbar}{\bar{\omega} \sqrt{2\pi}} \exp \left[ -\frac{1}{2} \left( \frac{\omega - \omega_0 - \Delta\omega}{\bar{\omega}} \right)^2 \right], \quad (9)$$

with  $\omega_0 = E_0/\hbar$ ,  $E_0$  being the vertical transition energy. The line shift  $\Delta\omega$  and the width  $\bar{\omega}$  are given as a function of the two first moments of the shifted Hamiltonians difference  $\Delta H = H_e - H_g - E_0$  by<sup>29</sup>

$$\hbar\Delta\omega = \langle \Delta H \rangle, \quad (10)$$

and

$$\hbar\bar{\omega} = \langle \Delta H^2 \rangle - \langle \Delta H \rangle^2. \quad (11)$$

We have noted here  $\langle A \rangle$  the thermal average of observable  $A$  over the ground state potential surface  $H_g$ . We now write the Hamiltonians  $H_g$  and  $H_e$  in harmonic (normal modes) coordinates  $\mathbf{Q}$ :

$$H_g = \frac{1}{2} \sum_i p_i^2 + \frac{1}{2} \mathbf{Q}^\dagger \mathbf{W}_g \mathbf{Q} \quad (12)$$

$$H_e = \frac{1}{2} \sum_i p_i^2 + \mathbf{G}^\dagger \mathbf{Q} + \frac{1}{2} \mathbf{Q}^\dagger \mathbf{W}_e \mathbf{Q} + E_0. \quad (13)$$

In these equations,  $\mathbf{W}_g$  is the mass-weighted Hessian matrix of the ground state at the lowest energy minimum  $\mathbf{Q}_0$ , which is assumed to be located at the origin  $\mathbf{0}$  of the reference frame.  $\mathbf{W}_g$  can be written as  $\mathbf{W}_g = \text{diag}(\omega_{g_i}^2)$ , as it is diagonal by construction.  $\mathbf{W}_e = (w_e^{ij})$  is the second derivatives matrix of the excited state surface at  $\mathbf{Q}_0$ . Lastly,  $\mathbf{G} = \partial H_e(\mathbf{Q}_0)/\partial \mathbf{Q}$  is the excited state gradient at  $\mathbf{Q}_0$ . The matrix  $\mathbf{W}_e$  is not assumed to be diagonal, and may include the so-called Duschinskii rotations.<sup>41</sup> It is then a simple matter of algebra to obtain the expressions for  $\Delta\omega$  and  $\bar{\omega}$ . Using the notation  $\rho_i = \omega_{g_i} \tanh \beta \hbar \omega_{g_i} / 2$ , we find

$$\Delta\omega = \frac{1}{4} \sum_i \frac{\omega_{g_i}^2 - w_e^{ii}}{\rho_i} \quad (14)$$

$$\bar{\omega}^2 = \frac{1}{8} \sum_i \left( \frac{\omega_{g_i}^2 - w_e^{ii}}{\rho_i} \right)^2 + \frac{1}{8} \sum_{i \neq j} \frac{(w_e^{ij})^2}{\rho_i \rho_j} + \frac{1}{2} \sum_i \frac{G_i^2}{\hbar \rho_i}$$

Apart from the different notations, the above expressions differ from the results by Wadi and Pollak by the second term in the right-hand side of Eq. (15), which was neglected by these authors.<sup>29</sup> Although Eqn. (14) and (15) are only valid for polyatomic, harmonic systems, anharmonic corrections can be carried out in the very same way as the perturbative expansion mentioned in the previous section and detailed in the Appendix. However, the present expressions are already the outcome of an approximation in the correlation function, hence we did not attempt to include such corrections here. In addition, their estimation would require the computation of higher order derivatives of the excited states energy surfaces, which will be a heavy numerical task, even for DIM potentials.

We have tested the Gaussian theory on small  $\text{CaAr}_n$  clusters. The ground- and excited-state Hamiltonians have been fully described previously.<sup>13</sup> They are based on the Diatomic-In-Molecules (DIM) formalism,<sup>42</sup> and were parameterized on *ab initio* calculations.<sup>30</sup> To give a better account of experimental properties of the  $\text{CaAr}$  diatomics, we have slightly modified the parameters with respect to our previous works.<sup>13,28</sup> The  $\text{Ca-Ar}$  ground state pairwise potential has been scaled by 0.85, and the excited state surfaces have been shifted by  $+305 \text{ cm}^{-1}$  to fit the  $4s4p$  experimental transition in calcium. As a consequence, some global minima may have changed, as in  $\text{CaAr}_{37}$ .

In the present work, we focus on the  $4s^2 \rightarrow 4s4p$  transitions, which have received some experimental attention.<sup>13</sup> The DIM Hamiltonian provides the energy and numerical derivatives, as well as the electronic transition dipole moment, for any atomic configuration  $\mathbf{R}$ . It can thus be used to simulate absolute absorption spectra. The ground state vibrational eigenmodes and eigenfrequencies  $\{\omega_{g_i}\}$  were obtained from the diagonalization of the Hessian matrix whose elements were computed from their analytical expressions. In both the classical and quantum cases, the absolute spectrum is calculated as the sum over the three possible excited states. For the Gaussian theory, the three gaussian curves are weighted by the square of the transition dipole moment at the equilibrium ground state geometry.

First, we have calculated the classical spectrum from the Gaussian theory in the classical limit  $\hbar \rightarrow 0$ , and from classical Metropolis Monte Carlo simulations at low temperature, using  $10^6$  cycles following  $2 \times 10^5$  equilibration cycles. The spectra of  $\text{CaAr}_{13}$  and  $\text{CaAr}_{54}$  at  $T = 5 \text{ K}$  are displayed in Fig. 1. For comparison, we have also plotted the predictions of the Gaussian theory in the classical limit  $\hbar \rightarrow 0$ . In this limit, the line shift and line width tend to their classical values  $(\hbar\Delta\omega)_c$  and  $(\hbar\bar{\omega})_c^2$  given respectively by

$$(\hbar\Delta\omega)_c = \frac{k_B T}{2} \sum_i \frac{\omega_{g_i}^2 - w_e^{ii}}{\omega_{g_i}^2}, \quad (16)$$

$$(\hbar\bar{\omega})_c^2 = \frac{(k_B T)^2}{2} \sum_i \left( \frac{\omega_{g_i}^2 - w_e^{ii}}{\omega_{g_i}^2} \right)^2 + \frac{(k_B T)^2}{2} \sum_{i \neq j} \frac{(w_e^{ij})^2}{\omega_{g_i} \omega_{g_j}} + k_B T \sum_i \frac{G_i^2}{\omega_{g_i}}. \quad (17)$$

The reliability of our comparison was checked by ensuring that only a single isomer was visited during the Metropolis MC simulation. As can be seen in Fig. 1, the accuracy of the Gaussian theory is very good at such low temperatures. The global minimum geometry of  $\text{CaAr}_{13}$  has two spectral lines located at  $23658$  (2 degenerate lines) and  $24034 \text{ cm}^{-1}$ , respectively. Due to its finite temperature, the cluster loses its instantaneous symmetry and the degeneracy is lifted. This explains why three distinct lines are seen in Fig. 1(a). In  $\text{CaAr}_{54}$  the Gaussian theory of absorption remains in good agreement with Monte Carlo data. This cluster has again 2 degenerate sharp lines at  $23715 \text{ cm}^{-1}$ , and one broad line at  $24080 \text{ cm}^{-1}$ . This time, the degeneracy is no longer lifted by temperature, and the two lines still merge into a single peak. In the classical theory the absorption intensity can also be obtained analytically by integrating Eq. (7) under the Condon assumption without performing the short-time expansion. Therefore, in the classical case, the differences between the calculated and simulated spectra in Fig. 1 can be attributed to anharmonicities only.

We now turn to a more complicated situation, namely  $\text{CaAr}_{37}$  in the quantum regime, and at moderate temperature  $T = 25 \text{ K}$ . We will show below that this temperature is located just above the melting point of this cluster. Many isomers are present, and this will provide a test of the superposition approximation. In the simulation, quantum effects have been included in a quasiclassical, corrective way by adding the corrective Feynman-Hibbs effective potential<sup>43</sup> to the ground state energy. This potential was shown to give good results on argon clusters with respect to the more accurate Fourier-path-integral Monte Carlo simulation of Neirotti and coworkers,<sup>44</sup> especially when compared with the alternative Wigner-Kirkwood corrections.<sup>45</sup> Since it is quasiclassical in nature, it cannot be used in the low temperature regime  $T \lesssim 5 \text{ K}$  where only few isomers are present, and path-integral simulations would have to be carried out instead. Because the superposition method does not assume any barrier nor pathway between the isomers, it yields supposedly ergodic data within the set of available minima. Therefore a reliable comparison with simulation results must also correct for possible broken ergodicity, and for this we have used parallel tempering Monte Carlo.<sup>25</sup> Also, since the effective potential explicitly depends on temperature, the probability of accepting an exchange between adjacent trajectories should be modified accordingly.<sup>46</sup>

Concerning the superposition approximation, and to quantify the importance of perturbative corrections in the partition function, we have separately considered zero-th order harmonic as well as second-order,

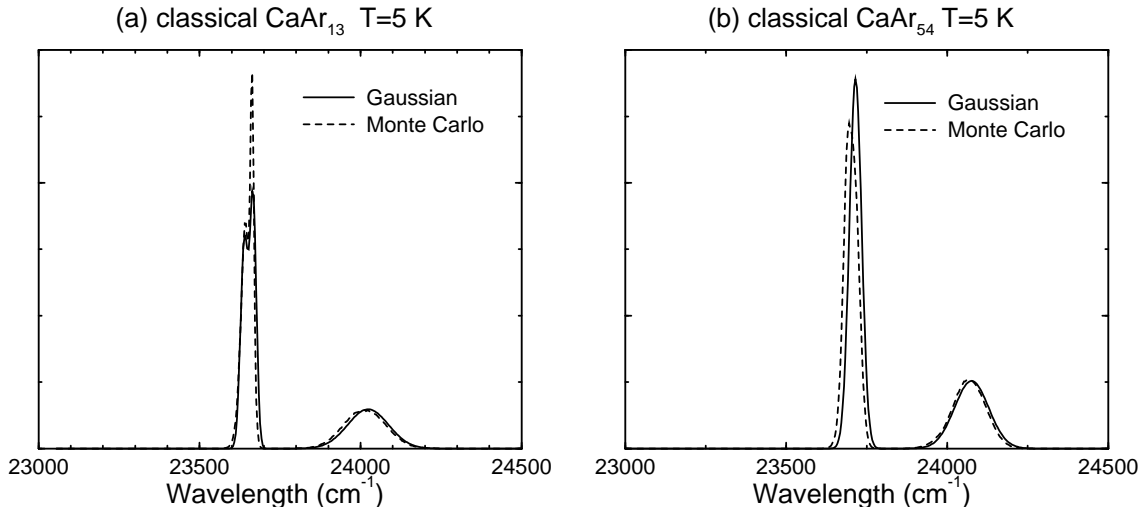


FIG. 1: Classical absorption spectra of the  $4s^2 \rightarrow 4s4p$  transition in (a)  $\text{CaAr}_{13}$  and (b)  $\text{CaAr}_{54}$  from Monte Carlo simulations (dashed lines) and the Gaussian theory (solid lines) at  $T = 5$  K.

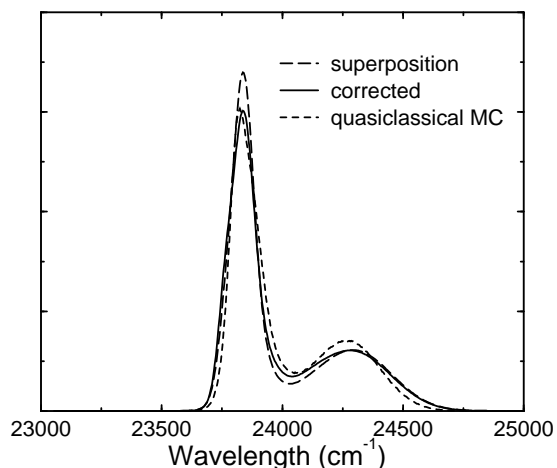


FIG. 2: Absorption spectra of  $\text{CaAr}_{37}$  at  $T = 25$  K from quasiclassical Monte Carlo simulations (dashed line) and the quantum superposition method in the harmonic approximation (long dashed line) or with anharmonic perturbative corrections (solid line).

anharmonic-corrected partition functions with the same database of isomers. The absorption spectra obtained with the Gaussian theory in the superposition approach and with quasiclassical MC simulations are represented in Fig. 2. The lowest energy isomer of this cluster, including the zero-point energy contribution, has three distinct spectral lines for the  $4s^2 \rightarrow 4s4p$  transition, namely at 23840, 23970, and 24260  $\text{cm}^{-1}$ . As can be seen from Fig. 2, none of these lines remain visible as peaks. We observe a very good agreement between the present theory and on-the-fly simulation, indicating that the relative weights of the isomers are correct. However, at this point,

we cannot tell whether the visible shifts and broadenings are an effect of temperature only, or of the different spectroscopic signatures of the other isomers present. Some shifts in the peaks remain slightly approximate in the superposition approach, and the second-order corrected weights only marginally improve the results. At 25 K, quantum effects turn out to be rather small on the line width and shape, but they may be more important on the weights of the isomers, as will be seen below. Therefore, from Fig 2 we see that anharmonic corrections to the isomers weights have a relatively weak influence for quasiclassical clusters. More information on the importance of these corrections will be gained by looking at the thermodynamical curves in the next section.

The Gaussian theory presented in this section can be extended to purely quantum systems at  $T = 0$ , for which delocalization is only due to the quantum nature of the vibrational modes, but not to an actual atomic displacement induced by a finite energy deposit. In this purpose, the Boltzmann weights in Eqn. (6) and (7) are replaced by the probability density of finding the system in its ground state at configuration  $\mathbf{R}$  as the square of the wavefunction. In the harmonic approximation, this probability density is a multidimensional Gaussian function, and the integrated absorption spectrum is found to be Gaussian with line shape and width given by the  $\beta \rightarrow \infty$  limits of Eqn. (14) and (15):

$$(\Delta\omega)_q = \frac{1}{4} \sum_i \frac{\omega_{g_i}^2 - \omega_e^{ii}}{\omega_{g_i}} \quad (18)$$

$$(\bar{\omega}^2)_q = \frac{1}{8} \sum_i \left( \frac{\omega_{g_i}^2 - \omega_e^{ii}}{\omega_{g_i}} \right)^2 + \frac{1}{8} \sum_{i \neq j} \frac{\omega_e^{ij}}{\omega_{g_i} \omega_{g_j}} + \frac{1}{2} \sum_i \frac{G_i^2}{\hbar \omega_{g_i}}. \quad (19)$$

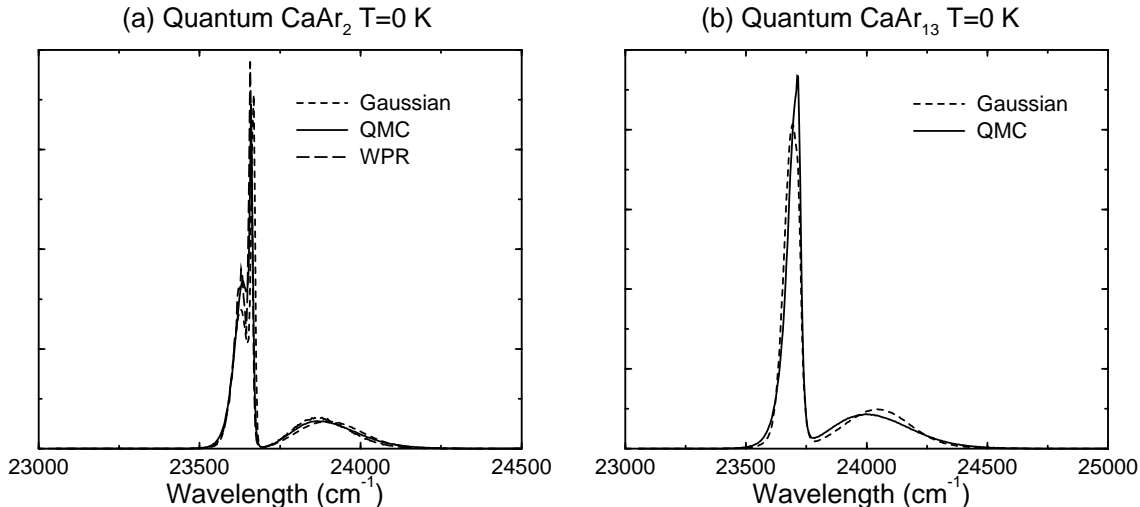


FIG. 3: Absorption spectra of (a)  $\text{CaAr}_2$  and (b)  $\text{CaAr}_{13}$  at  $T = 0$  K from diffusion Monte Carlo simulations (solid lines) and the Gaussian theory (dashed lines). For  $\text{CaAr}_2$ , we have also represented the results of wavepacket relaxation calculations (long dashed line).

The behavior of the Gaussian theory in the  $T = 0$  quantum case has been tested on  $\text{CaAr}_2$  and  $\text{CaAr}_{13}$  using simple diffusion Monte Carlo (DMC) in internal coordinates (without global rotation and translation), and without importance sampling. The DMC calculations were carried out with 1000 replicas, and the wave functions were averaged over  $10^5$  steps after  $10^5$  initial equilibration steps. In addition, for  $\text{CaAr}_2$ , the vibrational ground state wavefunction was also computed numerically on grids, using quantum wavepacket relaxation (WPR) method (imaginary time propagation).<sup>47</sup> The propagation was performed for zero total angular momentum, representing the wavepacket by an harmonic oscillator Discrete Variable Representation (DVR) for each of the two Ca–Ar bond coordinates, and by a Legendre DVR for the bending angle  $\widehat{\text{ArCaAr}}$ . The primitive basis for representing one bond coordinate includes 10 harmonic oscillator eigenfunctions. Associated Legendre functions with  $j < 60$  and  $m = 0$  were used for representing the bending mode. In both the DMC and WPR methods, which are both supposed to give essentially exact results, the absorption spectrum was calculated assuming vertical transitions from the quantum sample of geometries.

In Fig. 3 the absorption spectra calculated with these various methods are compared. For the small, triatomic cluster, the three methods give very similar peaks. In its equilibrium geometry,  $\text{CaAr}_2$  has three nondegenerate spectroscopic lines at 23621, 23670, and 23918  $\text{cm}^{-1}$ , respectively. Quantum delocalization of the vibrational modes leads to a rather small shift of these lines, and to a significant broadening. For  $\text{CaAr}_{13}$ , the simulated peaks are also in good agreement with the Gaussian prediction, but we notice that some asymmetry is visible on the “exact” spectrum from diffusion Monte Carlo. These effects

are clearly beyond a Gaussian description, and are due to anharmonic effects. These effects are relatively weak for the rather heavy calcium-doped argon clusters but may become more important for neon or helium clusters.

The above results suggest that the Gaussian theory of photoabsorption developed by Wadi and Pollak<sup>29</sup> upon the formal results of Yan and Mukamel<sup>40</sup> can give quite accurate results in both the classical and quantum regimes at low and moderate temperatures.

#### IV. SPECTROSCOPIC SIGNATURE OF PHASE CHANGES

The Gaussian theory described in the previous Section will now be used with the superposition approach to investigate the influence of temperature on the absorption spectra in context with isomerization phenomena.

For the two smallest clusters chosen,  $\text{CaAr}_6$  and  $\text{CaAr}_{10}$ , we performed extensive sampling of the ground state PES, and we believe that nearly all stable isomers have been identified. To apply the superposition method to larger  $\text{CaAr}_n$  clusters, the reweighting procedure from simulations must be used. Quasiclassical parallel tempering Monte Carlo simulations of  $10^7 + 2 \times 10^6$  equilibration cycles were used, for a set of temperatures equally spaced by 2.5 K in the range  $7.5 \text{ K} \leq T \leq 60 \text{ K}$  for  $n \leq 54$ , and  $15 \text{ K} \leq T \leq 75 \text{ K}$  for  $\text{CaAr}_{146}$ . The isomers were found by quenching the 50 K trajectory for all sizes except  $\text{CaAr}_{37}$ , for which the 25 K trajectory was used, and  $\text{CaAr}_{146}$ , quenched at 60 K. Local minimizations were performed every 500 cycles. To prevent evaporation, a rigid spherical container was used in the MC simulation.<sup>36,48</sup> The radii of the containers and the number of different isomers obtained from the quenches

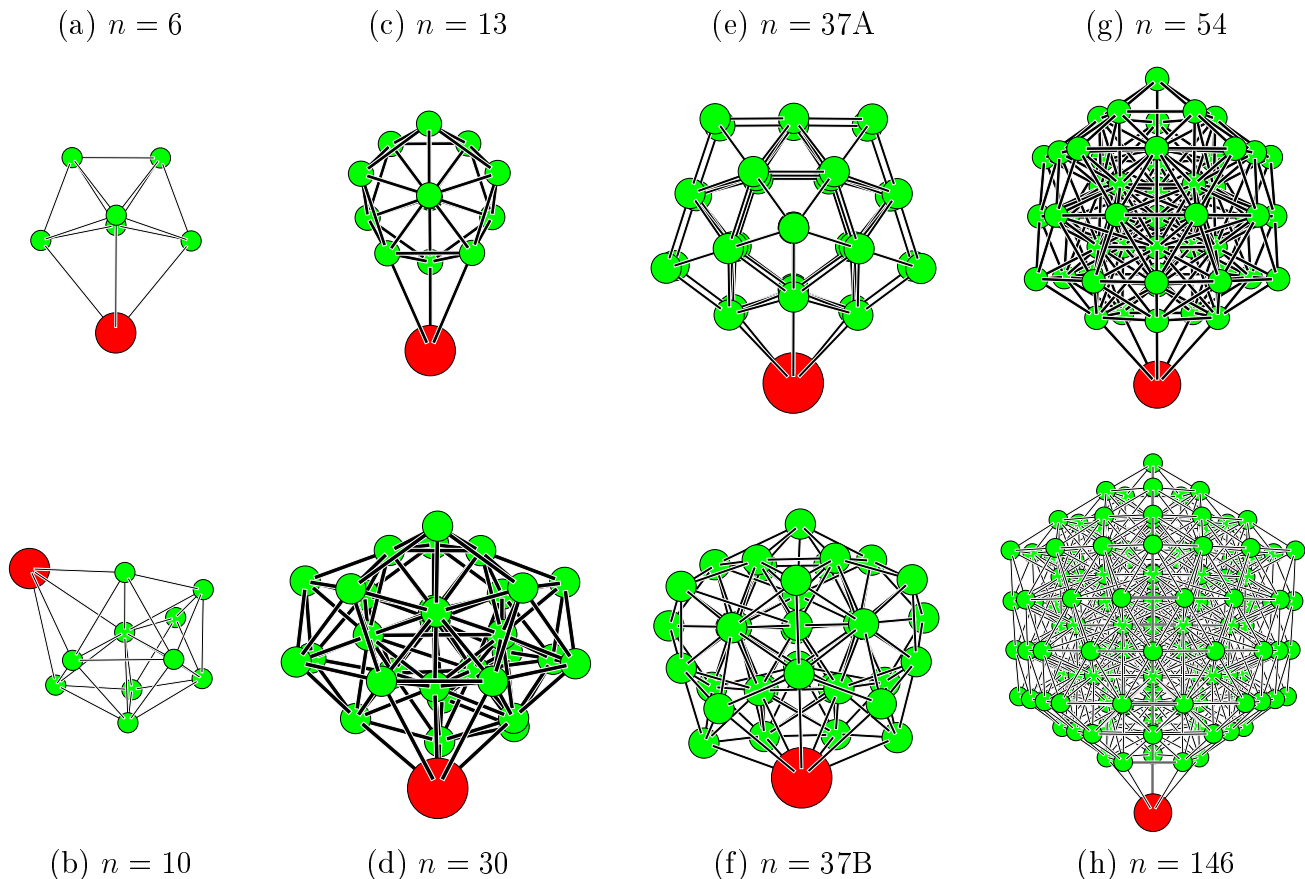


FIG. 4: Global minima of  $\text{CaAr}_n$  found by the basin-hopping algorithm after including the harmonic zero-point energy. (a)  $n = 6$ ; (b)  $n = 10$ ; (c)  $n = 13$ ; (d)  $n = 30$ ; (e)  $n = 37$ ; (f) second lowest energy minimum of  $\text{CaAr}_{37}$ ; (g)  $n = 54$ ; and (h)  $n = 146$ .

are given in Table I for the set of sizes chosen. We have also indicated the point group and energy of the global minima after including the zero-point harmonic contribution. These lowest-energy structures were generated from the basin-hopping or Monte Carlo + minimization algorithm.<sup>49</sup> They are shown in Fig. 4. In most cases, the global minimum of  $\text{CaAr}_n$  is very similar to the one of  $\text{Ar}_{n+1}$ , with one argon atom substituted by calcium. Due to the lower binding energy and larger equilibrium distance of  $\text{CaAr}$  with respect to  $\text{Ar}_2$ ,<sup>30</sup> calcium is always found on the surface of the remaining argon cluster. The nearly identical masses of calcium and argon atoms also induces relatively small changes in the vibrational properties, and the similarities between  $\text{CaAr}_n$  and  $\text{Ar}_{n+1}$  remain when including the zero-point corrections. However, in the case of  $\text{CaAr}_{37}$ , we find the somewhat surprising result that the global minimum geometry is decahedral, and remains so after including the harmonic zero point energy contribution. Slightly higher in energy, several icosahedral structures are found, either in the form of uncomplete multilayer icosahedra (Mackay type) or as polyicosahedra (anti-Mackay type). As in  $\text{Ar}_{38}$ , quantum delocalization favors anti-Mackay structures over Mackay

shapes,<sup>26</sup> yet a Mackay structure is found as the second isomer in both the classical and quantum regimes. This isomer is represented in Fig. 4(f). Additionally, the distorted truncated octahedron geometry lies above, but very close, to these isomers. As a consequence, the energy landscape of this particular cluster reveals interesting features, which will be investigated more deeply in the following article of this series.<sup>50</sup> This result is also consistent with the richer thermodynamical behavior generally observed in mixed van der Waals clusters with respect to homogeneous clusters.<sup>51,52</sup>

Therefore, even though  $\text{CaAr}_n$  and  $\text{Ar}_{n+1}$  clusters share many structural features, they also exhibit significant and unexpected differences, which could affect the thermodynamics and dynamics in large extents.

#### A. Isomerization in $\text{CaAr}_6$ and $\text{CaAr}_{10}$

The lowest energy minimum of  $\text{CaAr}_6$  is a distorted pentagonal bipyramid. The heat capacity of this cluster, computed from the superposition approach with or without anharmonic perturbative corrections, is repre-

TABLE I: Properties of the  $\text{CaAr}_n$  clusters simulated in this work. The energy and point group refer to the lowest energy minima, including the harmonic zero-point contribution.

Cluster size	Energy (eV/atom)	Point group	Container radius ( $\text{\AA}$ )	Quenching temperature (K)	Number of isomers
$\text{CaAr}_6$	0.02388	$C_{2v}$	6.348	–	12
$\text{CaAr}_{10}$	0.03192	$C_s$	7.935	–	391
$\text{CaAr}_{13}$	0.03721	$C_{3v}$	7.935	50	717
$\text{CaAr}_{30}$	0.04808	$C_1$	11.638	50	2347
$\text{CaAr}_{37}$	0.05044	$C_{4v}$	11.638	25	1444
$\text{CaAr}_{54}$	0.05690	$C_{5v}$	13.225	50	2563
$\text{CaAr}_{146}$	0.06695	$C_{5v}$	15.870	60	1690

sented in Fig. 5(a). For comparison, we have also plotted on the same curves the direct results of parallel tempering Monte Carlo with the Feynman-Hibbs effective potential.<sup>43</sup> As is well known for this potential,<sup>26</sup> the canonical heat capacity diverges upwards at low temperatures. Due to its small size, this cluster shows a nearly featureless caloric curve, and a flat heat capacity (except the low temperature increase) in Fig. 5(a). The small hump at  $T \sim 20\text{--}25$  K is indicative of isomerizations, and is followed by another bump near 45 K in the MC simulation. This latter broad peak is in fact spurious, as it comes from the dissociation of the weakly bound Ca atom. Previous works<sup>53,54</sup> have identified this peak as the signature of the liquid-vapor transition, from its dependence on the container radius. Here it would have been difficult to employ a radius smaller than  $6\text{\AA}$ , because the motion of argon atoms would have been hindered. The 25 K hump is barely visible, because it is hidden and smoothed out by quantum effects. The agreement between the superposition approximation and the quasiclassical MC simulations is very good except for the extra liquid-vapor bump. This feature is obviously missing from the assumptions made in the superposition method. The quantitative effect of perturbative corrections is small for this cluster.

$\text{CaAr}_{10}$  has the ground state of an uncomplete icosahedron. Some isomers involving different locations of the calcium atom lie not far above the global minimum, resulting in a shoulder in the heat capacity near 10–15 K in Fig. 5(b). The main peak near 30 K is due to a more complete rearrangement of argon atoms, and is reproduced quantitatively by the superposition approach after including perturbative corrections in the partition function.

The absorption spectra of these two clusters are represented in Fig. 5(c) and 5(d) as a function of temperature. In each of these figures, the classical spectra obtained from the limit  $\hbar \rightarrow 0$  has been superimposed to the quantum spectra. For the two sizes, the patterns are rather similar: the spectrum varies from a clear three-peak structure at low temperature towards a mostly single peak shape at high temperatures. The transition occurs roughly at 20 K in  $\text{CaAr}_6$ , and near 30 K in  $\text{CaAr}_{10}$ .

In the case of  $\text{CaAr}_6$  the high temperature main peak appears made of two smaller peaks, in agreement with simulations.<sup>55</sup> From a general point of view, quantum effects mainly consist in a broadening of the peaks. As expected, they get smaller and smaller as temperature increases, and becomes barely visible above 25 K.

Therefore, in these two small clusters, absorption spectroscopy seems to be an effective mean of detecting isomerization events, as the range of variation in the spectrum approximately matches the width of the heat capacity changes. As cluster size grows, one can thus expect to see sharper transitions, and to possibly use the calcium chromophore as a probe of the argon cluster melting point.

## B. Phase changes in $\text{CaAr}_n$ , $13 \leq n \leq 54$

We have chosen a set of sizes in the range  $13 \leq n \leq 54$ , spanning between 1 and 2 icosahedral layers, and which are likely to exhibit significant finite size effects. We first discuss the thermodynamical behavior of these clusters. The heat capacities obtained using the superposition method, with harmonic or second-order corrected anharmonic partition functions, are represented in Fig. 6 for the clusters corresponding to  $n = 13, 30, 37$ , and 54. In the case of the larger cluster  $\text{CaAr}_{54}$ , and also for  $\text{CaAr}_{146}$ , it was not possible to include all the required anharmonic corrections due to the too large computational requirements. Since they are not the main focus of the present paper, these thermodynamical data will be only briefly discussed in order to guide our interpretation of the following absorption spectra.

In general, we find again a rather good agreement between the quantum superposition results and the Monte Carlo simulations for all four sizes. As expected, anharmonic corrections do have a positive quantitative effect by bringing the superposition data closer to the simulation results. However, no new qualitative feature is visible when they are taken into account. All heat capacities exhibit a main peak indicative of the solidlike-liquidlike phase change.<sup>36</sup> This peak is located near 40–45 K for  $\text{CaAr}_{13}$ ,  $\text{CaAr}_{30}$  and  $\text{CaAr}_{54}$ , and near 20 K for



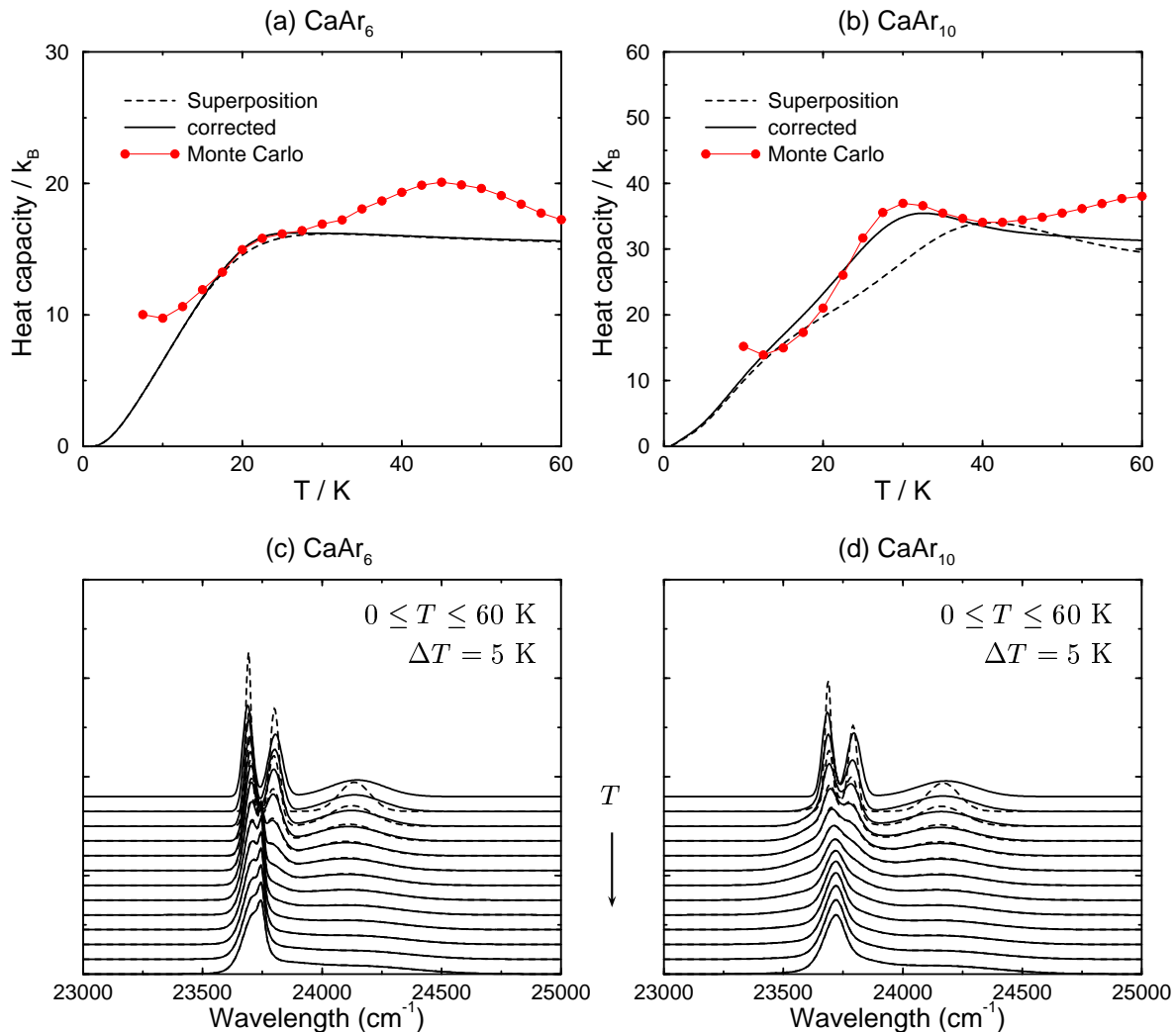


FIG. 5: Heat capacities computed from quasiclassical Monte Carlo simulations (full circles) and from the superposition method with harmonic (dashed lines) or anharmonic (solid lines) partition functions for (a)  $\text{CaAr}_6$  and (b)  $\text{CaAr}_{10}$ . Also represented are the finite-temperature absorption spectra calculated from the superposition method and the Gaussian theory of absorption in the quantum (solid lines) and classical (dashed lines) regimes for (c)  $\text{CaAr}_6$  and (d)  $\text{CaAr}_{10}$ .

$\text{CaAr}_{37}$ . This lower melting point is similar to what is observed in the 38-atom argon cluster described by the Lennard-Jones potential.<sup>56,57</sup> In addition to this main peak, extra humps or even peaks can be observed at lower temperatures in  $\text{CaAr}_{30}$  and  $\text{CaAr}_{37}$ . These features are indicative of preliminary isomerization resulting from solid-solid transitions in these clusters.<sup>58</sup> Again, they bear similarities with the known finite temperature behavior of LJ clusters with the same size.<sup>56,57,59,60</sup> In  $\text{CaAr}_{13}$ , the quantum character of the specific heat hides again a shoulder in the classical curve, as is the case in  $\text{CaAr}_6$ . This cluster happens to have a much larger number of stable isomers than  $\text{Ar}_{14}$ . In particular the capped icosahedron can be found with the calcium atom either in adatom location (lowest energy structure) or inside the icosahedral shell, resulting in a set of 4 different isomers slightly higher in energy. Structures not based on

the capped icosahedron, or with the calcium atom in the center of the icosahedron, are less stable than these five geometries. Therefore the energy spectrum of local minima can be put into three sets, one being the global minimum only, one being the other capped icosahedral isomers with calcium in the icosahedral shell, and all other isomers not build on the capped icosahedron motif. Because of these three sets, the melting process involves essentially two steps. In Fig. 7(a) we plot the probabilities of finding the  $\text{CaAr}_{13}$  cluster in its ground state, or in one of the 4 subsequent isomers, or in the remaining, liquid configurations. These probabilities are computed using the anharmonic corrected quantum partition functions. They display a clear two-step isomerization pattern. In the first step, at about 30 K, the calcium atom is able to leave its capping site in favor of one of the twelve icosahedral sites. Then, above 40 K, more disordered structures

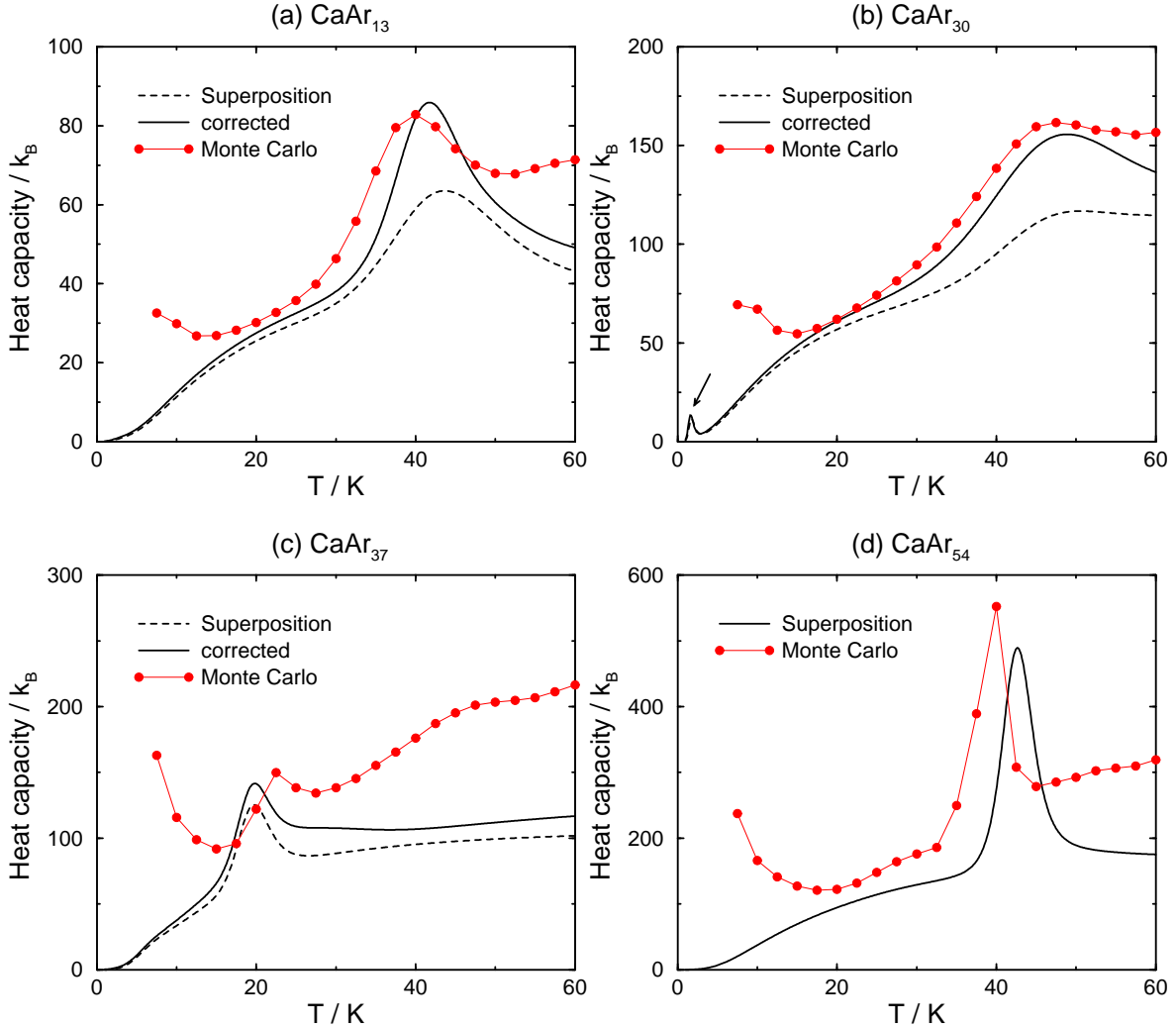


FIG. 6: Heat capacities of  $\text{CaAr}_n$  clusters. (a)  $n = 13$ ; (b)  $n = 30$ ; (c)  $n = 37$ ; and (d)  $n = 54$ . The notations are the same as in Fig. 5.

become thermally available the melting peak takes place.

In  $\text{CaAr}_{30}$  the preliminary solid-solid transition near 2.5 K involves polyicosahedral and multilayer icosahedral isomers, as in  $\text{Ar}_{31}$ .<sup>26,59</sup> Even though  $\text{CaAr}_{37}$  does not have the same global minimum as  $\text{Ar}_{38}$ , a similar thermodynamic behavior occurs. We have calculated from the harmonic superposition approximation the probabilities of finding the cluster either in its decahedral ground state isomer, in its (Mackay-type) icosahedral isomers, or in any of the remaining isomers. The variation of these probabilities with increasing temperature are displayed in Fig. 7(b). They show that the transition at about 5 K is due to a global decahedral-icosahedral rearrangement, and bears some similarity with the  $(\text{C}_{60})_{14}$  cluster.<sup>61</sup> The anti-Mackay and truncated octahedral structures are only marginally populated at thermal equilibrium, and the main heat capacity peak is associated with the emergence of a large number of disordered configurations. Hence it can be considered as the signature of melting.

For comparison, we have also plotted in Fig. 7(b) the corresponding curves in the classical limit. While the global behavior remains essentially unchanged, the preliminary transition occurs at a higher temperature, near 10 K.

The photoabsorption spectra of these clusters are represented in Fig. 8 for increasing temperatures in the range  $0 \leq T \leq 60$  K for all sizes except  $\text{CaAr}_{37}$ , for which  $0 \leq T \leq 40$  K. The classical spectra have also been plotted as dashed lines for  $T > 0$ . Except for  $\text{CaAr}_{37}$ , the classical spectrum looks very much like its quantum counterpart with slightly shifted but noticeably narrower excitation peaks. The four clusters display different absorption spectra, characteristic of finite-size effects. In  $\text{CaAr}_{13}$ , the spectrum gradually evolves from a two-peak structure (at about  $23700 \text{ cm}^{-1}$  and  $24100 \text{ cm}^{-1}$ ) to another two-peak structure (at about  $23650$  and  $23800 \text{ cm}^{-1}$ ). The peak ending at  $23800 \text{ cm}^{-1}$  appears first at 30 K, and originates from isomers where the Ca atom lies in the main icosahedral shell. No real signature of

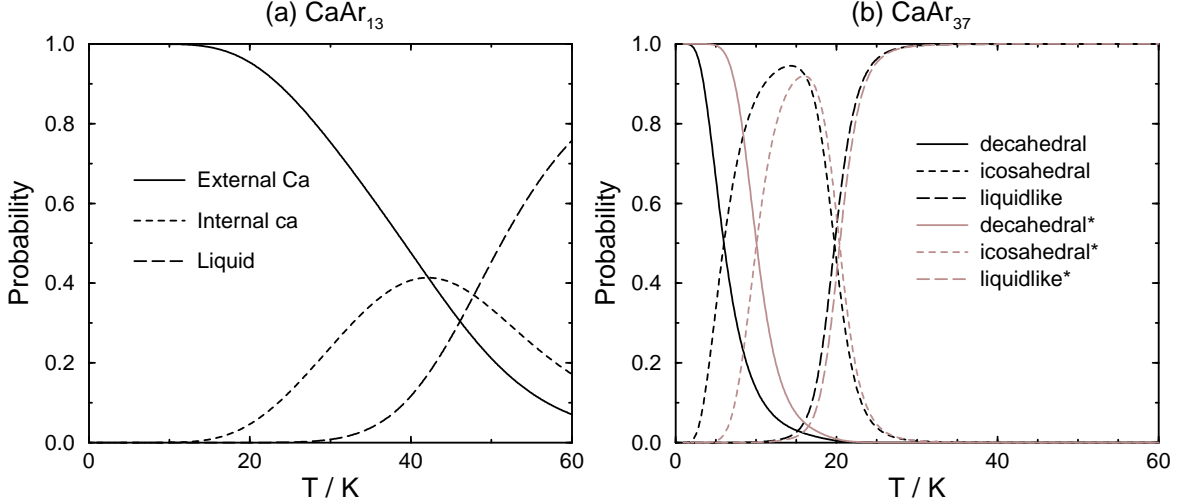


FIG. 7: (a) Probability to find the  $\text{CaAr}_{13}$  cluster with the calcium atom in a capping position (solid line), inside the icosahedral shell (dashed line), or in the liquidlike state (long dashed line). (b) Probability to find the  $\text{CaAr}_{37}$  cluster in its decahedral ground state (black solid line), in a Mackay-type icosahedral isomer (black dashed line), or in any other isomer (black long dashed line). The corresponding classical curves are also plotted as grey lines.

melting at 40 K is seen in Fig. 8(a), however the present spectra can still be interpreted in terms of isomerizations within the cluster.

In the case of  $\text{CaAr}_{30}$ , the low temperature isomerization below 5 K has a strong effect on the absorption peaks, which are red shifted by about 200 wavenumbers. The spectra of this cluster also evolves very continuously, and the two main peaks at  $23550$  and  $24000 \text{ cm}^{-1}$  undergo a slight red shift and thermal broadening. The weak melting phase change is reflected on these spectra, and the most prominent feature remains the sharp isomerization below 5 K.

Near  $T = 10$  K, the multiple peak structure of the spectrum in  $\text{CaAr}_{37}$  also reveals that several isomers are coexisting with distinct spectroscopic signatures. The solid-solid transition seen in the heat capacity of  $\text{CaAr}_{37}$  at low temperature is reflected on the absorption spectra in Fig. 8(c). The three-peak  $T = 0$  K spectrum is peculiar to the decahedral ground state. At  $T \sim 10$  K, a significant blue shift occurs in the middle peak, providing a signature of the icosahedral isomers. The quantitative difference in the solid-solid transition temperature induced by quantum effect is also seen in the absorption spectra between 5 and 15 K. Near 15 K, the spectrum can be clearly separated into more than three peaks, and suggests that distinct icosahedral isomers are present. At around 20 K, the various peaks merge into a double-peak structure, where the peak at  $23800 \text{ cm}^{-1}$  dominates the one at  $24750 \text{ cm}^{-1}$ . Here we find a clear thermodynamical influence on the spectroscopic properties. Hence, in this cluster, the absorption spectrum contains notable informations about isomerization and phase changes, including some rather fine details on the characteristic temperatures.

The equilibrium geometry of  $\text{CaAr}_{54}$  is a double layer Mackay icosahedron where the Ca atom is located on a vertex site, thus keeping a relatively high symmetry ( $C_{5v}$ ). As in  $\text{Ar}_{55}$ , the heat capacity near peak 40 K indicates volume melting,<sup>33,36</sup> while preliminary surface melting has a very small thermal signature. In Fig. 8(d) we observe that the two absorption peaks undergo a significant change near 30 K, and this corresponds to co-existing isomers with the Ca atom located on different substitutional sites of the external icosahedral shell. In this case the photoexcitation spectrum is sensitive to surface melting. At higher temperatures  $T > 40$  K, many isomers are found in which the metal atom is more fully solvated by argon. The spectra show another qualitative change, as the peak near  $23600 \text{ cm}^{-1}$  disappears and is replaced by a broad bump near  $24300 \text{ cm}^{-1}$ .

### C. $\text{CaAr}_{146}$

It is interesting to compare the situation in  $\text{CaAr}_{54}$  with the one in the larger Mackay icosahedron,  $\text{CaAr}_{146}$ . As in  $\text{CaAr}_{54}$ , the ground state equilibrium geometry has  $C_{5v}$  symmetry, with calcium located in a vertex site of the external icosahedral layer. This cluster has a huge number of isomers, and many high lying minima are missed during the quenching process. In the vast majority of structures in our sample the calcium atom remains in the outer argon layers. This is not surprising, since, and as was previously mentioned, the calcium-argon bond is weaker by about 70% than the argon-argon bond.<sup>13</sup> Despite the relatively small size of our sample with respect to the number of existing structures, the heat capacities in Fig. 9(a) exhibit a reasonably good agreement between

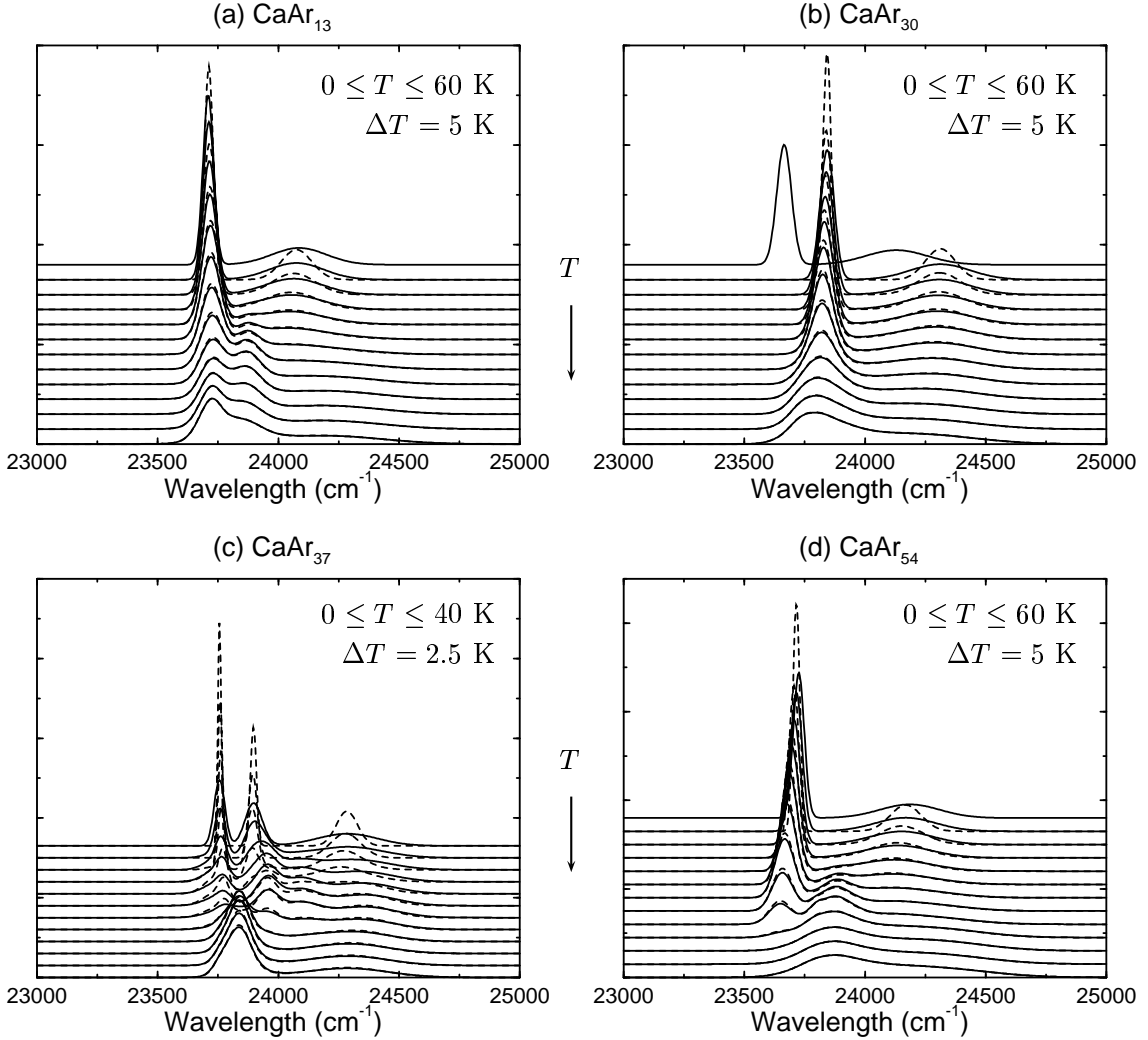


FIG. 8: Absorption spectra of the  $\text{CaAr}_n$  clusters corresponding to the heat capacities of Fig. 6. (a)  $n = 13$ ; (b)  $n = 30$ ; (c)  $n = 37$ ; and (d)  $n = 54$ . The notations are the same as in Fig. 5.

simulation and the superposition method, the high peak near 55 K being the signature of the solidlike-liquidlike phase change. Melting is essentially caused by the motion of argon atoms, and is relatively insensitive to the location of calcium. This explains the shape and the evolution of the absorption spectrum in Fig. 9(b). The two peaks at  $23720$  and  $24150 \text{ cm}^{-1}$  become broader and vanish between 25 K and 30 K, to be replaced by a major peak at  $23600 \text{ cm}^{-1}$ . This transition is correlated with fluctuations in the location of the calcium atom over the cluster surface. On the other hand, melting at 55 K does not lead to any visible change in the absorption spectrum.

#### D. Discussion

The above results may not be immediately amenable to experimental comparison, because of the problem of size selection. Our simulation results show that com-

plex isomerizations involving strong changes in the local environment of calcium could be, in principle, detected in experiments on size-selected clusters initially thermalized. However a typical sample of clusters in molecular beams is made of a broad size distribution, where the width and the center have values close to each other. The common feature of these clusters is the surface location of the calcium atom, and we may expect the absorption spectrum to be a possible probe of surface melting in these clusters, provided that the surface melting temperature does not significantly depend on cluster size. Even though calcium in bulk argon has a very distinct, three-peak spectroscopic signature,<sup>13</sup> it may be hard to detect volume melting in which calcium would be fully solvated. In fact, such van der Waals clusters evaporate atoms at temperature close to the melting point. From a statistical point of view, the weakly bonded calcium atom is likely to evaporate first. In addition the situations where calcium is fully solvated are less probable. Therefore the

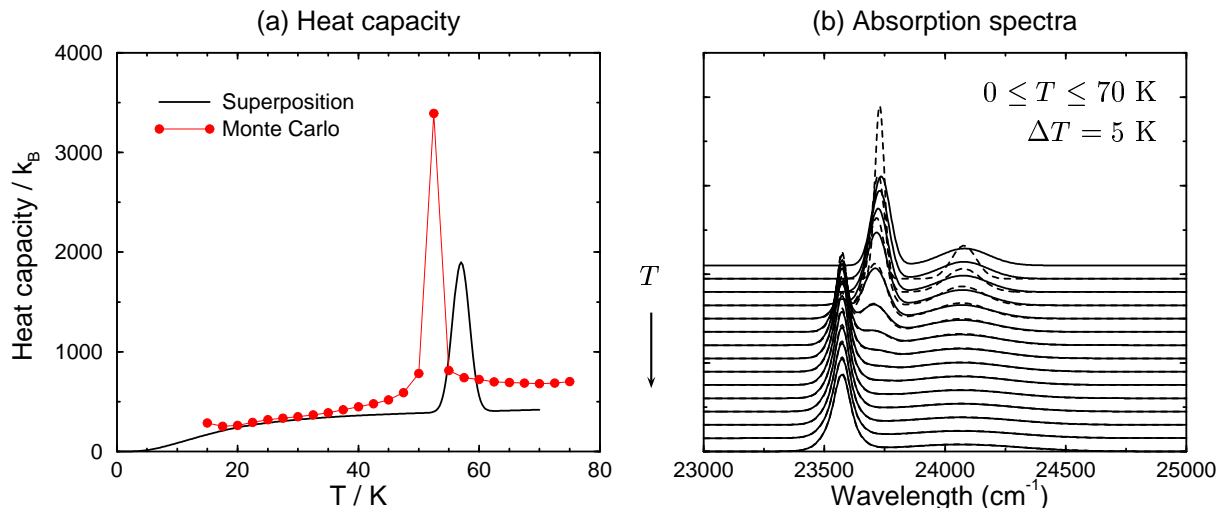


FIG. 9: (a) Heat capacity and (b) absorption spectra of  $\text{CaAr}_{146}$ . The notations are the same as in Fig. 5.

true volume melting transition occurring with full solvation of calcium may hardly be observed.

Provided that one could size-select these clusters, we have shown in the present work that spectroscopy can possibly probe their phase changes. More generally, intricate finite size effects in the thermodynamical behavior could be expected to be seen, as in  $\text{CaAr}_{13}$ ,  $\text{CaAr}_{30}$  or  $\text{CaAr}_{37}$ . In these special clusters, coexisting isomers and multiple phase-like induce complex variations of the absorption properties with increasing temperature.

Even with experimental setups involving selected sizes, another problem may come into play to hinder one from getting the complex spectroscopic information. All the above results are supposed to be at thermal equilibrium, without assuming how this equilibrium state had been reaching. In some cases, the relaxation time required for achieving equilibration may be very long because of multiple funnels in the energy landscape and kinetic trapping. This has been observed in the  $\text{Ar}_{38}$  cluster by Miller and coworkers,<sup>62</sup> where typical timescales of 10 s have been estimated for the interfunnel transitions at moderate temperatures. Relaxation to equilibrium and time-dependent absorption spectra will be the subject of the following article.<sup>50</sup>

## V. CONCLUSION

In this paper, we have investigated some methodological and practical aspects of finite temperature spectroscopy in chromophore-doped van der Waals clusters at thermal equilibrium. Using the harmonic superposition approach improved with anharmonic perturbation corrections to the partition function, the basic thermodynamical observables were calculated from samples of local minima on the energy landscape. The photoabsorption spectrum was obtained using the recent Gaussian

theory by Wadi and Pollak<sup>29</sup> in the harmonic approximation. These theories were tested and validated on selected  $\text{CaAr}_n$  clusters, in both the classical and quantum regimes, at low or moderate temperatures. Although anharmonic corrections could also be incorporated to the various quantities (line shifts and widths) in this theory, we found them unnecessary in the present work because of the other underlying approximations.

We have studied the possible spectroscopic signatures of the various isomerizations and phase changes in  $\text{CaAr}_6$ ,  $\text{CaAr}_{10}$ ,  $\text{CaAr}_{13}$ ,  $\text{CaAr}_{30}$ ,  $\text{CaAr}_{37}$ ,  $\text{CaAr}_{54}$ , and  $\text{CaAr}_{146}$ . The two smaller clusters show relatively simple isomerizations leading to a similar spectroscopic signature with a clear three- to one-peak pattern. Both  $\text{CaAr}_{30}$  and  $\text{CaAr}_{37}$  display strong (non monotonic) finite-size effects and solid-solid transitions. In  $\text{CaAr}_{13}$ , melting involves the calcium atom taking place of one argon atom in the icosahedral shell. In contrast with most other sizes, it is associated with the appearance of a new absorption peak. In  $\text{CaAr}_{54}$  and  $\text{CaAr}_{146}$ , preliminary surface melting occurs at nearly 30 K, and is reflected in the absorption spectrum. In all these phenomena, the local environment of calcium changes rather abruptly, resulting usually in clear shifts in some absorption peaks. Volume melting towards a calcium atom fully solvated by argon has a potentially significant spectral signature, however calcium is less bound to argon than argon itself, hence it is likely to dissociate before volume melting occurs. One should mention that the main heat capacity peak indicates melting of the argon cluster host, especially for large sizes. While the host cluster is liquidlike the calcium is still free, to some extent, to glide over the cluster surface. Being in this state, the rearrangements inside the argon cluster have little impact on the global spectroscopy of the chromophore, and the system can be expected to behave as a pseudo diatomics  $\text{Ca-Ar}_n$ . This point will be examined further in the third paper.<sup>66</sup>

The techniques used here are valid in both the quantum and classical regimes, which refers to the limit  $\hbar \rightarrow 0$ . They could be applied to other chromophore-doped van der Waals clusters, provided that potential energy surfaces are built first. In particular, neon clusters could be profitably investigated using the superposition method and the Gaussian theory of absorption. For helium, the harmonic approximation may break down, and even anharmonic corrections should be insufficient. In this case, quantum Monte Carlo should be coupled with on-the-fly histogram accumulation to compute the spectrum. More generally, the present methods are relevant to any statistical driven absorption spectrum in heterogeneous or homogeneous polyatomic molecules. For instance, the thermal effects on the absorption spectrum in small sodium clusters<sup>20,63</sup> could be investigated using appropriate models.<sup>64,65</sup> As concerns the approximations within the Gaussian theory, the most questionable point is the short-time expansion in the autocorrelation function. This approximation could be overcome using the formal results of Yan and Mukamel.<sup>40</sup> Unfortunately, this method involves a heavy numerical effort in the context of multiple isomers, and it still assumes harmonic forces. Finally, the superposition approximation provides a framework to study time-dependent properties over long time scales not available to molecular dynamics, by solving appropriate master equations.<sup>67</sup> The application of this technique to photoabsorption spectra will be made in the next paper of this series.<sup>50</sup>

### Acknowledgments

We thank CALMIP for a generous allocation of computer resources. FC also acknowledges interesting discussions with Dr. J. Vigué.

### APPENDIX: PERTURBATION EXPANSION OF THE PARTITION FUNCTION

The ground state Hamiltonian is written in cartesian coordinates  $\mathbf{P}, \mathbf{R}$  as  $H(\mathbf{P}, \mathbf{R}) = H_a(\mathbf{P}, \mathbf{R}) + \delta V(\mathbf{R})$ , where  $H_a$  is the harmonic term and  $\delta V$  the extra, anharmonic contribution. The Taylor expansion of  $\delta V$  near the minimum  $\mathbf{R}_0$  contains products of at least 3 coordinates. The partition function  $Z(\beta) = \text{Tr} \exp(-\beta H)$  is now expanded in a semiclassical fashion, in order to yield at least the same terms as the corresponding classical expansion. This approximation is actually correct from the quantum point of view as long as we keep it to first order. However, the rigorous perturbation treatment, which should be performed with path integrals, will not allow us to obtain the simple corrections that can be compared with the classical expressions of Ref. 39. Thus we write in a

phenomenological way

$$Z(\beta) \approx \text{Tr} \left[ e^{-\beta H_a} \prod_{n=0}^2 \frac{(-\beta)^n}{n!} (\delta V)^n \right], \quad (20)$$

and we keep only terms containing coordinates up to the power 12, which contribute to  $T^2$  corrections in the low-temperature classical partition function.<sup>39</sup> As in the classical case, all odd products have a zero contribution, but it is no longer possible to sort the various nonzero terms according to their power in  $\beta$ . It appears more natural to sort them according to the even power in coordinates. Following our previous notations<sup>39</sup> we write the anharmonic term  $\delta V$  as a function of the normal mode coordinates  $\mathbf{Q}$  as

$$\begin{aligned} \delta V(\mathbf{Q}) &= \sum_{k \geq 3} \frac{1}{k!} \sum_{i_1 \dots i_k} \left. \frac{\partial^k V}{\partial Q_{i_1} \dots \partial Q_{i_k}} \right|_{\mathbf{Q}=0} Q_{i_1} \times \dots \times Q_{i_k} \\ &= \sum_{k \geq 3} \frac{1}{k!} \sum_{i_1 \dots i_k} \Gamma_{i_1 \dots i_k}^{(k)} Q_{i_1} \times \dots \times Q_{i_k}. \end{aligned} \quad (21)$$

The corrective terms can be expressed as averages on the harmonic ground state:

$$Z(\beta) \approx Z_0(\beta)[1 + \gamma_4 + \gamma_6 + \gamma_8 + \gamma_{10} + \gamma_{12}], \quad (22)$$

where  $\gamma_i$  labels the correction due to power  $i$  in coordinates. These terms are explicitly given by

$$\begin{aligned} \gamma_4 &= -\frac{\beta}{24} \sum_{i_1 \dots i_4} \Gamma_{i_1 \dots i_4}^{(4)} \langle Q_{i_1} \times \dots \times Q_{i_4} \rangle; \\ \gamma_6 &= \sum_{i_1 \dots i_6} \left[ \frac{-\beta}{720} \Gamma_{i_1 \dots i_6}^{(6)} + \frac{\beta^2}{72} \Gamma_{i_1 i_2 i_3}^{(3)} \Gamma_{i_4 i_5 i_6}^{(3)} \right] \langle Q_{i_1} \times \dots \times Q_{i_6} \rangle; \\ \gamma_8 &= \sum_{i_1 \dots i_8} \left[ \frac{\beta^2}{1152} \Gamma_{i_1 \dots i_4}^{(4)} \Gamma_{i_5 \dots i_8}^{(4)} + \frac{\beta^2}{720} \Gamma_{i_1 i_2 i_3}^{(3)} \Gamma_{i_4 \dots i_8}^{(5)} \right] \langle Q_{i_1} \times \dots \times Q_{i_8} \rangle; \\ \gamma_{10} &= \sum_{i_1 \dots i_{10}} \left[ \frac{\beta^2}{28800} \Gamma_{i_1 \dots i_5}^{(5)} \Gamma_{i_6 \dots i_{10}}^{(5)} + \frac{\beta^2}{17280} \Gamma_{i_1 \dots i_4}^{(4)} \Gamma_{i_5 \dots i_{10}}^{(6)} \right. \\ &\quad \left. - \frac{\beta^3}{1728} \Gamma_{i_1 i_2 i_3}^{(3)} \Gamma_{i_4 i_5 i_6}^{(3)} \Gamma_{i_7 \dots i_{10}}^{(4)} \right] \langle Q_{i_1} \times \dots \times Q_{i_{10}} \rangle; \\ \gamma_{12} &= \sum_{i_1 \dots i_{12}} \left[ \frac{\beta^2}{1036800} \Gamma_{i_1 \dots i_6}^{(6)} \Gamma_{i_7 \dots i_{12}}^{(6)} - \frac{\beta^3}{51840} \Gamma_{i_1 i_2 i_3}^{(3)} \Gamma_{i_4 i_5 i_6}^{(3)} \Gamma_{i_7 \dots i_{12}}^{(6)} \right. \\ &\quad - \frac{\beta^3}{17280} \Gamma_{i_1 i_2 i_3}^{(3)} \Gamma_{i_4 \dots i_7}^{(4)} \Gamma_{i_8 \dots i_{12}}^{(5)} - \frac{\beta^3}{82944} \Gamma_{i_1 \dots i_4}^{(4)} \Gamma_{i_5 \dots i_8}^{(4)} \Gamma_{i_9 \dots i_{12}}^{(4)} \\ &\quad \left. + \frac{\beta^4}{31104} \Gamma_{i_1 i_2 i_3}^{(3)} \Gamma_{i_4 i_5 i_6}^{(3)} \Gamma_{i_7 i_8 i_9}^{(3)} \Gamma_{i_{10} i_{11} i_{12}}^{(3)} \right] \langle Q_{i_1} \times \dots \times Q_{i_{12}} \rangle. \end{aligned} \quad (23)$$

The above expressions can be considerably simplified by factorizing the average products  $\langle Q_i \times \dots \times Q_j \rangle$ . This is made possible by Wick's theorem, which holds for general bosonic ground states:

$$\langle Q_i^{2n} \rangle = \frac{1}{2^n} \frac{(2n)!}{n!} \langle Q_i^2 \rangle^n = (2n-1)!! \langle Q_i^2 \rangle^n, \quad (28)$$

with

$$\langle Q_i^2 \rangle = \frac{\hbar}{\omega_i} \left( \frac{1}{2} + \frac{1}{e^{\beta \hbar \omega_i} - 1} \right). \quad (29)$$

It is then more convenient to write the  $\gamma_i$ 's as diagrams, in which each  $k$ -vertex represents one of the  $\Gamma_{i_1 \dots i_k}^{(k)}$  term. For instance we have

$$\gamma_4 = -\frac{\beta}{8} \text{ (diagram of two ovals sharing a vertex)} \quad (30)$$

with

$$\text{ (diagram of two ovals sharing a vertex)} = \sum_{ij} \Gamma_{ij}^{(4)} \langle Q_i^2 \rangle \langle Q_j^2 \rangle. \quad (31)$$

The two diagrams giving  $\gamma_6$  are

$$\gamma_6 = -\frac{\beta}{48} \text{ (diagram of three ovals meeting at a central vertex)} + \frac{\beta^2}{8} \text{ (diagram of two ovals connected by a line)} + \frac{\beta^2}{12} \text{ (diagram of two ovals sharing a vertex with a line)}. \quad (32)$$

The other perturbative terms  $\gamma_8$ ,  $\gamma_{10}$ , and  $\gamma_{12}$  contain a larger number of diagrams, including non connected ones. The fewest diagrams are obtained in  $\ln Z$ , which still has 46 different contributions corresponding to Eq. (22):

$$\begin{aligned} \ln Z = \ln Z_0 & -\frac{\beta}{8} \text{ (diagram)} - \frac{\beta}{48} \text{ (diagram)} + \frac{\beta^2}{8} \text{ (diagram)} + \frac{\beta^2}{12} \text{ (diagram)} \\ & + \frac{\beta^2}{48} \text{ (diagram)} + \frac{\beta^2}{16} \text{ (diagram)} + \frac{\beta^2}{16} \text{ (diagram)} + \frac{\beta^2}{12} \text{ (diagram)} \\ & + \frac{\beta^2}{128} \text{ (diagram)} + \frac{\beta^2}{48} \text{ (diagram)} + \frac{\beta^2}{240} \text{ (diagram)} + \frac{\beta^2}{32} \text{ (diagram)} \\ & + \frac{\beta^2}{48} \text{ (diagram)} - \frac{\beta^3}{16} \text{ (diagram)} - \frac{\beta^3}{8} \text{ (diagram)} - \frac{\beta^3}{8} \text{ (diagram)} \\ & - \frac{\beta^3}{8} \text{ (diagram)} - \frac{\beta^3}{12} \text{ (diagram)} + \frac{\beta^2}{256} \text{ (diagram)} + \frac{\beta^2}{192} \text{ (diagram)} \\ & + \frac{\beta^2}{1440} \text{ (diagram)} - \frac{\beta^3}{64} \text{ (diagram)} - \frac{\beta^3}{24} \text{ (diagram)} - \frac{\beta^3}{32} \text{ (diagram)} \\ & - \frac{\beta^3}{32} \text{ (diagram)} - \frac{\beta^3}{16} \text{ (diagram)} - \frac{\beta^3}{72} \text{ (diagram)} - \frac{\beta^3}{32} \text{ (diagram)} \\ & - \frac{\beta^3}{8} \text{ (diagram)} - \frac{\beta^3}{48} \text{ (diagram)} - \frac{\beta^3}{32} \text{ (diagram)} - \frac{\beta^3}{8} \text{ (diagram)} \\ & - \frac{\beta^3}{12} \text{ (diagram)} - \frac{\beta^3}{24} \text{ (diagram)} - \frac{\beta^3}{24} \text{ (diagram)} - \frac{\beta^3}{16} \text{ (diagram)} \\ & - \frac{\beta^3}{48} \text{ (diagram)} - \frac{\beta^3}{48} \text{ (diagram)} - \frac{\beta^3}{24} \text{ (diagram)} - \frac{\beta^3}{32} \text{ (diagram)} \\ & - \frac{\beta^3}{48} \text{ (diagram)} + \frac{\beta^4}{16} \text{ (diagram)} + \frac{\beta^4}{16} \text{ (diagram)} + \frac{\beta^4}{48} \text{ (diagram)} \end{aligned}$$

$$\begin{aligned}
& + \frac{\beta^4}{8} \begin{array}{c} \bullet \\ \diagup \quad \diagdown \\ \bullet \quad \bullet \\ \diagdown \quad \diagup \\ \bullet \end{array} + \frac{\beta^4}{24} \begin{array}{c} \bullet \\ \diagup \quad \diagdown \\ \bullet \quad \bullet \\ \diagdown \quad \diagup \\ \bullet \end{array} \quad . \quad (33)
\end{aligned}$$

It is important to notice that this perturbative expansion includes all 18 terms up to second-order in the classical expansion,<sup>39</sup> and that 28 remaining terms would contribute classically to 3rd and higher orders in  $T^n$ . These terms correspond to the  $\Gamma^{(5)} \times \Gamma^{(5)}$ ,  $\Gamma^{(4)} \times \Gamma^{(6)}$ ,  $\Gamma^{(3)} \times \Gamma^{(4)} \times \Gamma^{(5)}$ , and  $\Gamma^{(4)} \times \Gamma^{(4)} \times \Gamma^{(4)}$  products, but cannot be neglected a priori with respect to the other

corrections in the quantum regime.

In the superposition method framework, these perturbative corrections act on the individual partition functions, where they are expected to give a more accurate estimate of the relative weights of the isomers as a function of temperature, as well as more accurate thermodynamical observables.

- <sup>1</sup> C. Gée, M. A. Gaveau, J. M. Mestdagh, M. A. Osborne, O. Sublimontier, and J. P. Visticot, *J. Phys. Chem.* **100**, 13421 (1996).
- <sup>2</sup> J. M. Mestdagh, M. A. Gaveau, C. Gée, O. Sublimontier, and J. P. Visticot, *Int. Rev. Phys. Chem.* **16**, 215 (1997).
- <sup>3</sup> M. A. Gaveau, C. Gée, J. M. Mestdagh, and J. P. Visticot, *Comments At. Mol. Phys.* **34**, 241 (1999).
- <sup>4</sup> R. Baumfalk, N. H. Nahler, U. Buck, M. Y. Niv, and R. B. Gerber, *J. Chem. Phys.* **113**, 329 (2000).
- <sup>5</sup> P. Slavicek, P. Zdanska, P. Jungwirth, R. Baumfalk, and U. Buck, *J. Phys. Chem. A* **104**, 7793 (2000).
- <sup>6</sup> R. Baumfalk, N. H. Nahler, and U. Buck, *Faraday Discuss.* **118**, 247 (2001).
- <sup>7</sup> M. A. Gaveau, M. Briant, P. R. Fournier, J. M. Mestdagh, and J. P. Visticot, *Phys. Chem. Chem. Phys.* **2**, 831 (2000).
- <sup>8</sup> Z. Liu, H. Gómez, and D. M. Neumark, *Faraday Discuss.* **118**, 221 (2001).
- <sup>9</sup> M. Briant, M. A. Gaveau, P. R. Fournier, J. M. Mestdagh, J. P. Visticot, and B. Soep, *Faraday Discuss.* **118**, 209 (2001).
- <sup>10</sup> W. H. Breckenridge, P.-R. Fournier, M.-A. Gaveau, J.-M. Mestdagh, and J.-P. Visticot, *Chem. Phys. Lett.* **364**, 225 (2002).
- <sup>11</sup> J. P. Visticot, J. Berlande, J. Cuvellier, A. Lallement, J. M. Mestdagh, P. Meynadier, P. de Pujo, and O. Sublimontier, *Chem. Phys. Lett.* **191**, 107 (1992).
- <sup>12</sup> J. P. Visticot, P. de Pujo, J. M. Mestdagh, A. Lallement, J. Berlande, O. Sublimontier, P. Meynadier, and J. Cuvellier, *J. Chem. Phys.* **100**, 158 (1994).
- <sup>13</sup> M. A. Gaveau, M. Briant, P. R. Fournier, J. M. Mestdagh, J. P. Visticot, F. Calvo, S. Baudrand, and F. Spiegelman, *Euro. Phys. J. D* **21**, 153 (2002).
- <sup>14</sup> M. Y. Hahn and R. L. Whetten, *Phys. Rev. Lett.* **61**, 1190 (1988).
- <sup>15</sup> U. Even, N. Ben-Horin, and J. Jortner, *Phys. Rev. Lett.* **62**, 140 (1989).
- <sup>16</sup> R. S. Berry, J. Jellinek, and G. Natanson, *Chem. Phys. Lett.* **107**, 227 (1984).
- <sup>17</sup> M. R. Ghayal and E. Curotto, *J. Chem. Phys.* **111**, 5522 (1999).
- <sup>18</sup> A. M. Aguado and E. Curotto, *Chem. Phys. Lett.* **330**, 440 (2000).
- <sup>19</sup> J. H. Skone and E. Curotto, *J. Chem. Phys.* **117**, 7137 (2002).
- <sup>20</sup> M. Moseler, H. Hakkinen, and U. Landman, *Phys. Rev. Lett.* **87**, 053401 (2001).
- <sup>21</sup> M. Grigorov and F. Spiegelmann, *Surf. Rev. Lett.* **3**, 211 (1996).
- <sup>22</sup> J. Galindez, F. Calvo, P. Paska, D. Hrivnak, R. Kalus, F. X. Gadéa, *Comp. Phys. Comm.* **145**, 126 (2002).
- <sup>23</sup> D. J. Wales, J. P. K. Doye, M. A. Miller, P. N. Mortenson, and T. R. Walsh, *Adv. Chem. Phys.* **115**, 1 (2000).
- <sup>24</sup> B. A. Berg and T. Neuhaus, *Phys. Rev. Lett.* **68**, 9 (1991).
- <sup>25</sup> C. J. Geyer, in *Computing Science and Statistics: Proceedings of the 23rd Symposium on the Interface*, American Statistical Association, (New York, 1991), p. 156; E. Marinari and G. Parisi, *Europhys. Lett.* **19**, 451 (1992).
- <sup>26</sup> F. Calvo, J. P. K. Doye, and D. J. Wales, *J. Chem. Phys.* **114**, 7312 (2001).
- <sup>27</sup> J. P. K. Doye and D. J. Wales, *J. Chem. Phys.* **102**, 9659 (1995).
- <sup>28</sup> F. Calvo, J. P. K. Doye, and D. J. Wales, *Chem. Phys. Lett.* **366**, 176 (2002).
- <sup>29</sup> H. Wadi and E. Pollak, *J. Chem. Phys.* **110**, 11890 (1999).
- <sup>30</sup> F. Spiegelman, L. Maron, W. H. Breckenridge, J.-M. Mestdagh and J.-P. Visticot, *J. Chem. Phys.* **117**, 7534 (2002).
- <sup>31</sup> M. R. Hoare, *Adv. Chem. Phys.* **40**, 49 (1979).
- <sup>32</sup> F. H. Stillinger and T. A. Weber, *Phys. Rev. A* **25**, 978 (1982).
- <sup>33</sup> D. J. Wales, *Mol. Phys.* **78**, 151 (1993).
- <sup>34</sup> G. Franke, E. R. Hilf, and P. Borrmann, *J. Chem. Phys.* **98**, 3496 (1993).
- <sup>35</sup> F. H. Stillinger, *Phys. Rev. E* **59**, 48 (1999).
- <sup>36</sup> P. Labastie and R. L. Whetten, *Phys. Rev. Lett.* **65**, 1567 (1990).
- <sup>37</sup> K. D. Ball and R. S. Berry, *J. Chem. Phys.* **109**, 8541 (1998).
- <sup>38</sup> J. Cao and G. A. Voth, *J. Chem. Phys.* **102**, 3337 (1995); **103**, 4211 (1995); D. R. Reichman and G. A. Voth, *ibid.* **112**, 3267 (2000); **112**, 3280 (2000).
- <sup>39</sup> F. Calvo, J. P. K. Doye, and D. J. Wales, *J. Chem. Phys.* **115**, 9627 (2001).
- <sup>40</sup> Y. J. Yan and S. Mukamel, *J. Chem. Phys.* **85**, 5908 (1986).
- <sup>41</sup> F. Duschinskii, *Acta. Physicochim. URSS* **7**, 551 (1937).
- <sup>42</sup> P. J. Kuntz and J. Valdorf, *Z. Phys. D* **8**, 195 (1988).
- <sup>43</sup> R. P. Feynman and A. R. Hibbs, *Quantum mechanics and path integrals* (McGraw-Hill, New York, 1965).
- <sup>44</sup> J. P. Neirotti, D. L. Freeman, and J. D. Doll, *J. Chem. Phys.* **112**, 3990 (2000).



- <sup>45</sup> E. Wigner, Phys. Rev. **40**, 749 (1932); J. G. Kirkwood, *ibid.* **44**, 31 (1933).
- <sup>46</sup> F. Calvo and F. Spiegelman, Phys. Rev. Lett. **89**, 266401 (2002).
- <sup>47</sup> R. Kosloff and H. Tal-Ezer, Chem. Phys. Lett. **127**, 223 (1986).
- <sup>48</sup> J. K. Lee, J. A. Barker, and F. F. Abraham, J. Chem. Phys. **58**, 3166 (1973).
- <sup>49</sup> D. J. Wales and J. P. K. Doye, J. Phys. Chem. A **101**, 5111 (1997).
- <sup>50</sup> F. Calvo, F. Spiegelman, and D. J. Wales, second paper of this series.
- <sup>51</sup> D. D. Frantz, J. Chem. Phys. **105**, 10030 (1996); **106**, 1992 (1997).
- <sup>52</sup> L. J. Munro and K. D. Jordan, Comp. Phys. Comm. **145**, 1 (2002).
- <sup>53</sup> M. Moseler and N. Nordiek, Phys. Rev. B **60**, 11734 (1999).
- <sup>54</sup> F. Calvo, J. Phys. Chem. B **105**, 2183 (2001).
- <sup>55</sup> F. Calvo, F. Spiegelman, M.-A. Gaveau, M. Briant, P. R. Fournier, J.-M. Mestdagh, and J.-P. Visticot, submitted to Euro. Phys. J. D.
- <sup>56</sup> J. P. K. Doye and D. J. Wales, Phys. Rev. Lett. **80**, 1357 (1998); J. P. K. Doye, D. J. Wales, and M. A. Miller, J. Chem. Phys. **109**, 8143 (1999); J. P. K. Doye, M. A. Miller, and D. J. Wales, *ibid.* **110**, 6896 (1999).
- <sup>57</sup> J. P. Neirotti, F. Calvo, D. L. Freeman, and J. D. Doll, J. Chem. Phys. **112**, 10340 (2000); F. Calvo, J. P. Neirotti, D. L. Freeman, and J. D. Doll, *ibid.* **112**, 10350 (2000).
- <sup>58</sup> J. P. K. Doye and F. Calvo, J. Chem. Phys. **116**, 8307 (2002).
- <sup>59</sup> F. Calvo and J. P. K. Doye, Phys. Rev. E **63**, 010902(R) (2001).
- <sup>60</sup> D. D. Frantz, J. Chem. Phys. **115**, 6136 (2002).
- <sup>61</sup> F. Calvo, J. P. K. Doye, and D. J. Wales, Phys. Rev. Lett. **87**, 119301 (2001).
- <sup>62</sup> M. A. Miller, J. P. K. Doye, and D. J. Wales, Phys. Rev. E **60**, 3701 (1999).
- <sup>63</sup> M. Schmidt, C. Ellert, W. Kronmüller, and H. Haberland, Phys. Rev. B **59**, 10970 (1999); M. Schmidt and H. Haberland, Euro. Phys. J. D **6**, 109 (1999).
- <sup>64</sup> R. Poteau and F. Spiegelmann, Phys. Rev. B **45**, 1878 (1991).
- <sup>65</sup> R. Poteau, D. Maynau, and F. Spiegelmann, Chem. Phys. **175**, 289 (1993).
- <sup>66</sup> F. Calvo, F. Spiegelman, and J.-M. Mestdagh, third paper of this series.
- <sup>67</sup> N. G. van Kampen, *Stochastic Processes in Physics and Chemistry* (North-Holland, Amsterdam, 1981).